FLOW CONTROL OVER A RAMP USING ACTIVE VORTEX GENERATORS.

C. Cuvier[1,2], **C. Braud**[1,3], **J.M. Foucaut**[1,2], **M. Stanislas**[1,2]
Univ Lille Nord de France[1] F-59000 Lille, EC Lille[2], CNRS[3],
Laboratoire de Mécanique de Lille (UMR 8107)
Boulevard Paul Langevin,
59655 Villeneuve d'Ascq Cédex, France.
christophe.cuvier@gmail.com
caroline.braud@univ-lille1.fr
jean-marc.foucaut@ec-lille.fr
michel.stanislas@ec-lille.fr

ABSTRACT

A parametric study of separation control using continuous jets vortex generators was conducted on a two-dimensional ramp with a mild adverse pressure gradient on a 2 m flat plate and a flow separation on a flap. Two jets diameters were investigated : 6 and 12 mm. For both diameters, co and counter-rotating arrangements were analysed. The control efficiency was quantified by wool-tufts visualisations and by four friction probes placed on the flap. It was found that a skewness of the output voltage of a friction probe greater than -0.4 is characteristic of flow reattachment. Different spacing between jets, different pitch angles, different distances of the jets to the separation line and different VR were tested. The best configuration obtained is a counter-rotating one, with $\frac{\Phi}{\delta} = 0.03$, $\frac{\lambda}{\Phi} = 27.3$, $\frac{L}{\Phi} = 15$ and $\alpha = 135°$.

Key words : Turbulent boundary layers, adverse pressure gradient, flow separation, control, continuous jets.

INTRODUCTION

Turbulent Boundary Layer (TBL) separation induces by strong adverse pressure gradient (APG) or by sudden discontinuity of curvature can lead to a drop in efficiency of a turbomachinery or to a loss of aircraft control. In a way of improving continuously the performances and the safeness of all the machineries that interact with fluids (aircraft, turbomachineries, cars, etc.), preventing and/or controlling turbulent boundary layer flow separation seems to be a crucial point that has to be solved.

Since the beginning of the 1990s, many studies were performed on flow separation control (see Lin et al., 1990; Lin et al., 1991; Lin, 1999; Selby et al., 1992; McManus et al., 1994; Godard and Stanislas, 2006a; Godard and Stanislas, 2006b; etc.). Flow separation control experiments can be classified in two types. The first one corresponds to passive control strategies (Lin et al., 1990; Lin et al., 1991; Lin, 1999; Godard and Stanislas, 2006a; etc.). The second one concerns active control (Selby et al., 1992; McManus et al., 1994; Godard and Stanislas, 2006b; etc.). The active control strategies can be divided also in two families. The first one concerns steady continuous jets vortex generators (VGs) (Selby et al., 1992; Godard and Stanislas, 2006b; etc.), and the second one concerns unsteady VGs (like pulsed-jets in McManus et al., 1994; etc.). Good reviews of control strategies can be found in GadelHak (2000) and Lin (2002).

For real flow control applications, it seems that the active strategies are the most appropriate as on an aircraft, the actuators can be turned off when they are not necessary, to avoid any additional drag and reactive control (closed-loop) can be achieved. Round jets are popular active VGs (Godard and Stanislas, 2006b; Selby et al., 1992; McManus et al., 1994; etc.). Their control efficiency depends on many parameters such as the diameter, the orientation, the exit velocity, the arrangement (co or counter-rotating), etc. (see Compton and Johnston, 1991 or Godard and Stanislas, 2006b). Moreover, the flow where the actuators is embedded has significant influence on the control results as the adverse pressure gradient tends to increase interactions between vortices and thus decrease the control efficiency (Lin, 2002). This explains the existing disagreement between investigators on the optimal active control parameters.

The experiment presented here was performed on a two dimensional ramp, designed for the AVERT (Aerodynamic Validation of Emission Reducing Technologies) FP6 EC project. The ramp was tuned such as a boundary layer with mild adverse pressure gradient develops on the 2 m flat plate. At the end of this flat plate, there is an imposed separation with a flap which is used to quantified the control efficiency.

THE EXPERIMENT

The wind tunnel facility and the ramp

This parametric active control experiment has been conducted in the LML boundary layer wind tunnel at $U_\infty = 10$ m/s. A boundary layer develops on the 20 m long lower wall

to reach around 30 cm at the end. This thick boundary layer allows good spatial resolution. The test section is 2 m span and 1 m height and the free-stream velocity is ranging from 1 to 10 m/s ($\pm 0.5\%$). In this experiment, the wind tunnel was used in close-loop configuration to allow temperature regulation ($\pm 0.2°C$). For detailed characteristics of the wind tunnel, see Carlier and Stanislas (2005).

The ramp model was mounted on the wind tunnel floor such as the beginning of the ramp was 14.4 m downstream of the entrance of the test section. Figure 1 gives a schematic view of the ramp. It is composed of four parts. The first one is a smooth converging part with a contraction ratio of 0.75. The second part is an articulated flat plate of more than 2 m. The angle between this plate and the wind tunnel floor is called α and is counted positive if it corresponds to a positive rotation around the z axis (Figure 1). The angle α tunes the pressure gradient of the boundary layer that develops on the 2.1 m flat plate. α is ranging from $2°$ to $-4°$. The third part of the ramp is an other articulated flat plate (called flap). The angle between this plate and the wind tunnel floor is called β and its sign used the same convention as α. β is ranging from $-5°$ to $-40°$. The aim of the flap is to allow to create and fix a flow separation. The angle β tunes the strength and the extend of the flow separation. The last part is a flexible plate to allow smooth connection between the end of the flap and the floor of the wind tunnel.

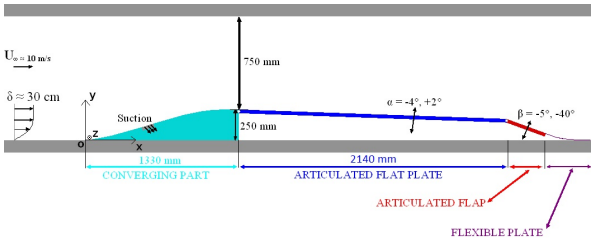

Figure 1. Schematic view of the ramp.

In the present study, the angles α and β were fixed at respectively $-2°$ and $-22°$. This configuration corresponds to an adverse pressure gradient on the flat plate and a separation on the flap. It was characterized carefully with wall pressure measurements and by 5 hot-wire profiles on the flat plate. Details about the flow characterization of the ramp can be found in Cuvier et al. (2010) and in Cuvier et al. (2011). Figure 2 gives the pressure gradient distribution along the ramp and Table 1 gives the main boundary layer parameters. The separation begin at the flap articulation at $s = 3500$ mm (With s the curvilinear coordinate of the ramp with O as origin (Figure 1)).

Experimental techniques

Different measurement techniques were used to quantified the control efficiency on flow separation.

Wool tufts visualisations Wool tufts visualisations were used on the flap to check visually the separation and its extend. Several lines of wool tufts of 4 cm long were

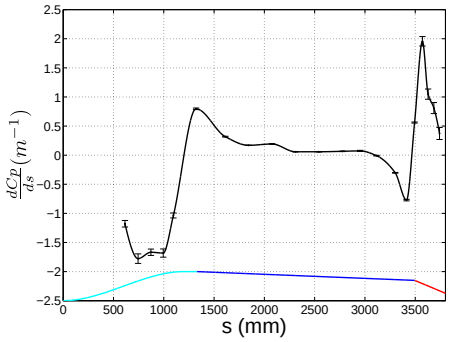

Figure 2. Streamwise pressure gradient distribution, for $\alpha = -2°$, $\beta = -22°$ and $U_\infty = 10$ m/s.

Table 1. Boundary layer characteristics at $U_\infty = 10$ m/s, $\alpha = -2°$, $\beta = -22°$.

St	s (mm)	δ (cm)	δ^* (mm)	θ (mm)	Re_θ
St1	1508	17.4	14.4	12.2	10100
St2	1974	19.6	16.5	13.7	10600
St3	2440	20.3	17.9	14.7	11700
St4	2968	21.2	20.3	16.5	12600
St5	3382	19.0	16.4	13.5	10100

St	H	U_e (m/s)	u_τ (m/s)	$(\frac{\partial P}{\partial s})^+$ $(\times 10^3)$	$\beta_{Clauser}$
St1	1.18	12.9	0.482	3.28	1.44
St2	1.21	12.6	0.459	1.47	0.70
St3	1.22	12.5	0.462	0.46	0.24
St4	1.23	12.4	0.435	0.67	0.38
St5	1.21	12.3	0.465	-5.54	-2.56

placed on all the span of the flap and on the flexible plate. The length of the separation is about 80 cm (Figure 3). An example of wool tufts visualisation with a complete suppression of separation by control is shown in Figure 4.

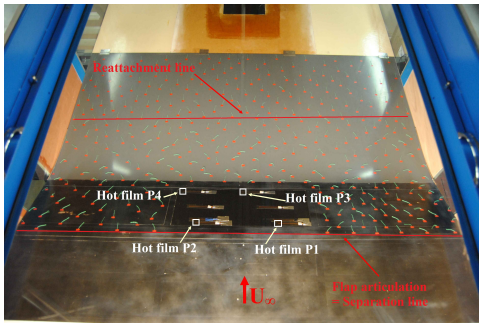

Figure 3. Wool tufts visualisation of the separation, $\alpha = -2°$, $\beta = -22°$ and $U_\infty = 10$ m/s.

Hot-film friction probes The control effects are assessed quantitatively using four friction probes placed on the flap. The coordinates of these probes are given in Table 2

Figure 4. Example of wool tufts visualisation with control and no separation, $\alpha = -2°$, $\beta = -22°$ and $U_\infty = 10$ m/s.

and are shown in Figure 3. The friction probes that were used are Senflex SF9902 hot film probe. They are 1.5 mm long and they are deposited on a polyamyde substrate with a thickness less than 0.2 mm. They can be glued directly on the surface with 60 μm double-sided tape. As was introduced by Godard and Stanislas (2006a), a hole of 2 mm in diameter and 1 mm in depth was drilled under the sensor to minimize heat losses to the substrate. The probes were connected to a 4 channels AN 1003 anemometer manufactured by AAlabSystems. The acquisition frequency was 11 kHz and the cut-off frequency 5 kHz. Fifteen packets of 10 s were acquired for each measurement to achieve good convergence of the mean value, standard deviation, PDF and spectrum.

An in-situ calibration of the hot film friction probes was not possible. A pseudo calibration based on the calibrations done by Godard and Stanislas (2006b) for the same type of probes was developed. The King's law is for these probes : $E^2 = E_0^2 + b.\tau^n$, where E is the output voltage of the bridge, and τ the wall friction. The parameters to be estimated are E_0, b and n. The pseudo calibration consists in estimating the coefficient of the King's law with $E_{0_{wts}}$, that corresponds to the output voltage of the bridge when the wind tunnel is stopped and at the temperature of calibration ($T_{calibration}$). For all calibrations done by Godard, the value $\left(\frac{E_0}{E_{0_{wts}}}\right)^2$ and $\frac{b}{E_{0_{wts}}^2}$ were computed. It appears that these two values remain almost constants and equal respectively to 0.91 and 0.52. So by measuring only $E_{0_{wts}}$, an estimated value of E_0 and b can be obtained. The parameter n was taken as $\frac{1}{3}$ as Godard found it constant and equal to this value.

A lot of configurations were acquired without control at different temperatures and on different days, to check the repeatability of the method. It can reached around $\pm 10\%$ on different days and $\pm 5\%$ on the same day.

Table 2. Coordinates of the friction probes.

probe	P1	P2	P3	P4
s (mm)	3555	3555	3759	3759
z (mm)	164	-205	0	-286

Hot film friction probes are not sensitive to the flow direction, so they give the absolute value of the wall friction $|\tau|$. The criterion to detect the separation is not as easy as $\tau < 0$ corresponds to separated flow and $\tau > 0$ to attached flow. The criterion that was used to detect separation was build with the variation of $|\tau|$ and the variation of the skewness of the output voltage of the bridge. For flow without control, the PDF of the output voltage of the bridge is not Gaussian and this signal has a skewness between -0.8 and -0.7. When the flow is completely attached (that was verified with wool tufts visualisations), the PDF of the output voltage of the bridge tends to be Gaussian. The skewness is between -0.4 and 0. A skewness greater than -0.4 was then considered as an attached flow.

Flow rate regulation and quantification circuit The jets were supplied with filtered and dried compressed air through a regulation and quantification circuit and a 90 liters tank. The compressed air circuit is provided with a pressure regulator and a progressive valve to allow to tune the flow rate. The flow rate is measured by an adequate vortex meter. Finally, the pressure and the temperature of the compressed air are measured to access the density. The regulation and quantification circuit allows to measure the mass flow rate of the jets at less than $\pm 2\%$ for $2 \leq Q_v \leq 560\ m^3/h$.

Tests description

Figures 5 and 6 illustrate the definition of the different parameters of the jets. The jets parameters tested were chosen based on the study of Godard and Stanislas (2006b). Two diameters of jets were tested : 6 and 12 mm, corresponding respectively to $\frac{\Phi}{\delta} = 0.03$ and 0.06. Both co-rotating and counter-rotating arrangements were used. The skew angle β (see Figures 5 and 6) was fixed at 45°, and two values of the pitch angle α (see Figures 5 and 6) were tested : $\alpha = 45°$ (downstream blowing) and $\alpha = 135°$ (upstream blowing). Tests were performed at two distances from the separation line : $s = 3383$ mm (station 1) and $s = 3219$ mm (station 2). These stations correspond to $\frac{\Delta X_{vg}}{\delta} = 0.6$ and 1.4, with ΔX_{vg} the distance between the jets position and the separation line ($s = 3500$ mm). At station 1, $\delta = 19$ cm and at station 2, δ was estimated at 20.2 cm.

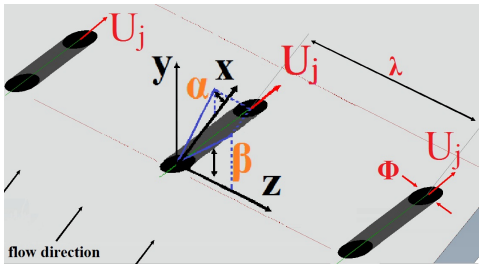

Figure 5. Co-rotating jet parameters.

For the co-rotating configurations, for each jet diameter, two values of $\frac{\lambda}{\Phi}$ were tested : 6.8 and 13.6 for $\Phi = 12$ mm, and 13.6 and 27.2 for $\Phi = 6$ mm. For $\Phi = 12$ mm, and upstream blowing, $\frac{\lambda}{\Phi} = 20.4$ and 27.2 were also tested. For the counter-rotating configurations, two values of $\frac{\lambda}{\Phi}$ were tested : 27.3 and 54.6. The $\frac{L}{\Phi}$ parameter was chosen as 15. For $\Phi = 12$ mm,

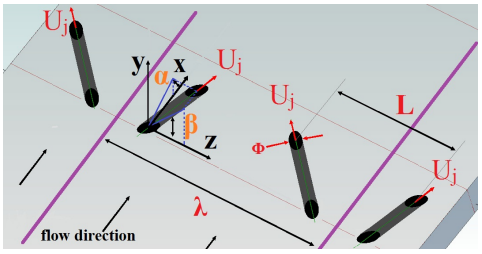

Figure 6. Counter-rotating jet parameters.

$\frac{L}{\Phi} = 12.3$ was also tested.

The velocity ratio VR tested for each configuration varies between 0.5 and 3.5 by steps of 0.5. VR is defined by $VR = \frac{U_{mean}}{U_e}$, where U_{mean} is the mean jets exit velocity and U_e the local free-stream velocity. For $\Phi = 12$ mm, it was found that $U_j = 1.2U_{mean}$ and for $\Phi = 6$ mm, it was found that $U_j = 1.236U_{mean}$, with U_j the maximum exit velocity of the jets. The differences between jets were checked. For VR between 0.5 to 5, it was found less than $\pm 10\%$ differences on the maximum jet exit velocity for $\Phi = 12$ mm and $\pm 2\%$ for $\Phi = 6$ mm. The actuators were placed on the full 2 m span of the ramp. Tables 3 and 4 give a summary of all the tests that were carried out. Each configuration tested (i.e. one Φ, one α, one $\frac{\Delta X_{vg}}{\Phi}$ one $\frac{\lambda}{\Phi}$ and one $\frac{L}{\Phi}$) has been numbered case 1 to 44. More details can be found in Cuvier et al. (2010).

Table 3. List of the co-rotating control cases tested.

Φ	β	α	$\frac{\Delta X_{vg}}{\Phi}$	$\frac{\lambda}{\Phi}$	VR
6	45	45, 135	19.5, 46.8	13.6, 27.2	0.5-3.5
12	45	45, 135	9.8, 23.4	6.8, 13.6[1]	0.5-3.5

Table 4. List of the counter-rotating control cases tested.

Φ	β	α	$\frac{\Delta X_{vg}}{\Phi}$	$\frac{\lambda}{\Phi}$	$\frac{L}{\Phi}$	VR
6	45	45, 135	19.5, 46.8	27.3, 54.6	15	0.5-3.5
12	45	45, 135	9.8, 23.4	27.3, 54.6	12.3, 15	0.5-3.5

RESULTS AND DISCUSSION

For all the tests carried out, for the same vortex generators (VGs) configuration at $\frac{\Delta X_{vg}}{\delta} = 0.6$ and 1.4, no difference was observed. Maybe the investigated values of $\frac{\Delta X_{vg}}{\delta}$ were to small to make a difference as Godard and Stanislas (2006b) found that active jets VGs are efficient for $\frac{\Delta X_{vg}}{\delta} = 7.2$ and Lin et al. (1990) for $\frac{\Delta X_{vg}}{\delta} = 40$, so much further away. It can also be concluded that there is no effect of $\frac{\Delta X_{vg}}{\Phi}$ in the investigated interval (i.e. between 9.8 to 46.8).

Figures 7 and 8 give respectively the gain in friction and the skewness with VR, versus the spanwise position z,

[1]For $\alpha = 135°$, $\frac{\lambda}{\Phi} = 20.4$ and 27.2 were also tested.

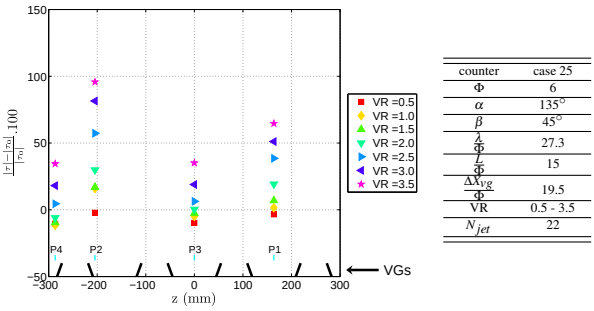

counter	case 25
Φ	6
α	135°
β	45°
$\frac{\lambda}{\Phi}$	27.3
$\frac{L}{\Phi}$	15
$\frac{\Delta X_{vg}}{\Phi}$	19.5
VR	0.5 - 3.5
N_{jet}	22

Figure 7. Gain in friction for case 25 and different VR.

for case 25, corresponding to a counter-rotating configuration with $\Phi = 6$ mm, $\alpha = 135°$, $\frac{\lambda}{\Phi} = 27.3$, $\frac{L}{\Phi} = 15$ and $\frac{\Delta X_{vg}}{\delta} = 0.6$. The position of the friction probes used (Table 2) are represented. A schematic view of the jets axis position projected in (oyz) plane is represented at the bottom of the figures. The beginning of the lines corresponds to the spanwise jets position. In all the following figures, the same scale is used to allow comparisons between the different cases. For case 25, the skewness (so the efficiency of control) continuously increases with VR for probes P1 and P2. For probes P3 and P4, it increases after $VR = 2.5$. This means that the separation is first delayed and then suppressed. The same behaviour is observed on the gain in friction (Figure 7). At $VR = 3.5$, the separation is totally suppressed and, for all the friction probes, the skewness is constant around -0.2, but the gain in friction is not constant. This explains the choice of the skewness as a criterion rather than the gain in friction.

Using only wool tufts visualisations, an optimum of VR higher than 3.5 was looked for in case 25. At VR around 10 the separation was also totally suppressed. For all the test cases with upstream blowing ($\alpha = 135°$), the same behaviour as case 25 was observed. For upstream blowing, the efficiency of control continuously increases with VR, however, to obtain visible effects on the wool tufts, a value of VR greater than 1.5 is needed. This is in agreement with previous study of Godard and Stanislas (2006b), Betterton et al. (2000), McManus et al. (1994) and Selby et al. (1992).

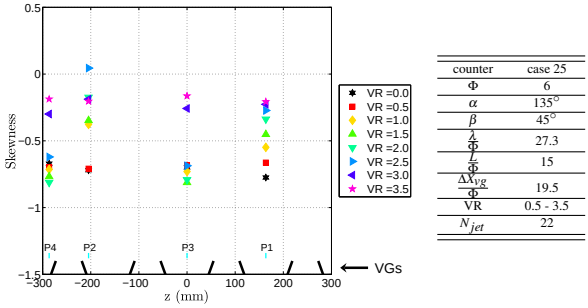

counter	case 25
Φ	6
α	135°
β	45°
$\frac{\lambda}{\Phi}$	27.3
$\frac{L}{\Phi}$	15
$\frac{\Delta X_{vg}}{\Phi}$	19.5
VR	0.5 - 3.5
N_{jet}	22

Figure 8. Skewness for case 25 and different VR.

Figure 9 gives the skewness for different VR, versus the

spanwise position z, for case 27. This case differs from case 25 only by α ($\alpha = 45°$, i.e. downstream blowing). In this case, to obtain visible effects on the wool tufts, a value of VR greater than 1.5 is also needed. The skewness increases with VR (probe P1 and P2) until $VR = 1.5 - 2.5$, then it decreases. It seems then that there is an optimum VR between 1.5 and 2.5 for downstream blowing. This is surprising as it seems to has never been observed. Upstream blowing appears then to be more robust than downstream blowing as VR can be continuously increased to increase the control efficiency.

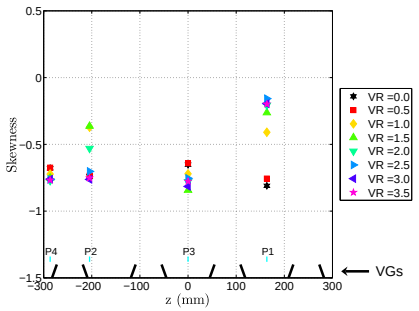

counter	case 27
Φ	6
α	45°
β	45°
$\frac{\lambda}{\Phi}$	27.3
$\frac{L}{\Phi}$	15
$\frac{\Delta X_{vg}}{\Phi}$	19.5
VR	0.5 - 3.5
N_{jet}	22

Figure 9. Skewness for case 27 and different VR.

For the co-rotating cases with $\frac{\lambda}{\Phi} = 6.8$, the control results were contentious as the wool tufts took the jets direction. An other flow is then created that does not correspond to a good control result. The parameter $\frac{\lambda}{\Phi}$ for co-rotating VGs has to be greater than 6.8. Figure 10 gives the skewness for case 7 with $VR = 2.5$ and for case 8 with $VR = 3.5$. The scheme of the jets corresponds to case 8. These cases correspond to co-rotating upstream blowing configurations with $\Phi = 6$. The result are almost the same. For case 7 and $VR = 2.5$, $Q_{v_7} = 69m^3/h$ and $C_{\mu_7} = 0.023$, and for case 8 and $VR = 3.5$, $Q_{v_8} = 48m^3/h$ and $C_{\mu_3} = 0.024$, with Q_v the volumetric flow rate and C_μ the momentum coefficient ($C_\mu = \frac{\rho_{jet}.N_{jet}.S_{jet}.U^2_{mean}}{\frac{1}{2}.\rho_e.\Delta z.\delta.U^2_e}$, with ρ_{jet} the density of the jet, ρ_e the density in the wind tunnel, N_{jet} the number of jets, S_{jet} the cross section of a jet, Δz the span of control and δ the boundary layer thickness). Case 8 with $\frac{\lambda}{\Phi} = 27.2$ seems to give better result at constant Q_v or C_μ, however, to obtain a complete suppression of the separation for case 8, a velocity ratio of 5.5 is needed, which is unrealistic for aircraft or car applications. For the other tests of $\frac{\lambda}{\Phi}$ for the co-rotating arrangement, almost the same results were obtained. It was concluded that the optimum value of $\frac{\lambda}{\Phi}$ is about 13.6 for co-rotating VGs that is two times greater than Godard and Stanislas (2006b) one.

For the counter-rotating VGs, the cases with $\frac{\lambda}{\Phi} = 54.6$ need a VR greater than 6 in upstream blowing configuration to suppress totally the separation, which is unrealistic. For the corresponding cases with downstream blowing, no total suppression of the separation was achieved. It was concluded that $\frac{\lambda}{\Phi} = 27.3$ is the best value for counter-rotating jets.

Figure 11 gives the skewness for case 21 and 37 with $VR = 3.5$. The difference between these two cases is the parameter $\frac{L}{\Phi}$. The scheme of the jets corresponds to case 37. Case 37 gives better result. The parameter $\frac{L}{\Phi} = 12.3$ is then

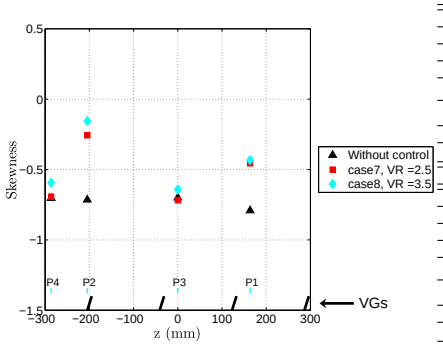

co	case 7
Φ	6
α	135°
β	45°
$\frac{\lambda}{\Phi}$	13.6
$\frac{\Delta X_{vg}}{\Phi}$	19.5
VR	2.5
N_{jet}	22

co	case 8
Φ	6
α	135°
β	45°
$\frac{\lambda}{\Phi}$	27.2
$\frac{\Delta X_{vg}}{\Phi}$	19.5
VR	3.5
N_{jet}	11

Figure 10. Skewness for case 7 and $VR = 2.5$, and for case 8 and $VR = 3.5$.

better than 15. However, no result is observed on probe P3. The spacing between two pairs of VGs are too large. The value of $\frac{\lambda}{\Phi}$ has then to be reduced. This suggests that the optimum value of $\frac{\lambda}{\Phi}$ has to be smaller than $2\frac{L}{\Phi}$. The parameter $\frac{L}{\Phi} = 12.3$ seems to be better than 15, but as $\frac{\lambda}{\Phi}$ has to be decreased to obtain a spanwise uniform control, more jets are needed, so more flow rate. The configuration $\frac{\lambda}{\Phi} = 27.3$ and $\frac{L}{\Phi} = 15$ is then an efficient compromise and can be considered near optimum. The optimum interval between 12.5 and 16 for $\frac{L}{\Phi}$ found by Godard and Stanislas (2006b) is then confirmed by the present study.

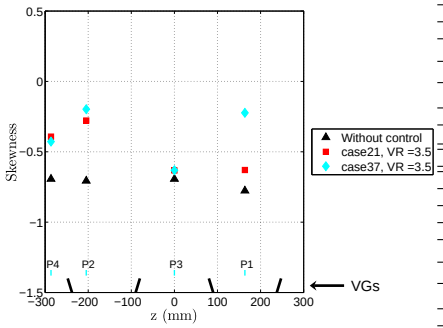

counter	case 21
Φ	12
α	135°
β	45°
$\frac{\lambda}{\Phi}$	27.3
$\frac{L}{\Phi}$	15
$\frac{\Delta X_{vg}}{\Phi}$	9.8
VR	3.5
N_{jet}	10

counter	case 37
Φ	12
α	135°
β	45°
$\frac{\lambda}{\Phi}$	27.3
$\frac{L}{\Phi}$	12.3
$\frac{\Delta X_{vg}}{\Phi}$	9.8
VR	3.5
N_{jet}	12

Figure 11. Skewness for case 21 and 37, $VR = 3.5$.

The effects of the parameter $\frac{\Phi}{\delta}$ was also investigated. At constant VR, except for the co-rotating configurations with $\Phi = 12$ mm and upstream blowing, for all the configurations investigated, the configurations with $\frac{\Phi}{\delta} = 0.03$ give better or comparable results. Looking at the flow rate or C_μ, as between $\frac{\Phi}{\delta} = 0.06$ and $\frac{\Phi}{\delta} = 0.03$ configurations, the total cross section is divided by 2, for all the configurations tested, the parameter $\frac{\Phi}{\delta} = 0.03$ is the best one.

Figure 12 compares the results of the optimum counter-rotating and the optimum co-rotating configuration found. The counter-rotating gives better results. Finally, for the same jets diameter, the optimum co and counter-rotating configurations have the same number of jets for 2 m span.

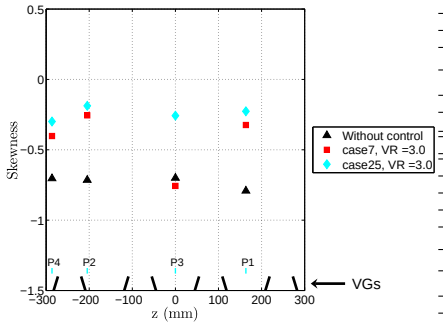

co	case 7
Φ	6
α	135°
β	45°
$\frac{\lambda}{\Phi}$	13.6
$\frac{\Delta X_{vg}}{\Phi}$	19.5
VR	3
N_{jet}	22

counter	case 25
Φ	6
α	135°
β	45°
$\frac{\lambda}{\Phi}$	27.3
$\frac{L}{\Phi}$	15
$\frac{\Delta X_{vg}}{\Phi}$	19.5
VR	3
N_{jet}	22

Figure 12. Skewness for case 7 and 25, $VR = 3$.

CONCLUSIONS

A parametric study of active jets VGs base on the study of Godard and Stanislas (2006b) has been conducted on a ramp with a mild adverse pressure gradient and a flow separation on a flap. Both counter and co-rotating arrangements were tested. Two diameters of jets were analysed : $\Phi = 6$ and 12 mm. The control efficiency is characterized by wool tufts visualisations and four friction probes on the flap. The adapted reattachment criterion for friction probes is a skewness of the output voltage greater than -0.4.

It results that there is no effect of $\frac{\Delta X_{vg}}{\delta}$ in the investigated interval between 0.6 and 1.4. The minimum of VR to obtain visible effects on wool tufts is 1.5. For upstream blowing, it was found that the efficiency of control continuously increased with VR, whereas for downstream blowing an optimum exist between 1.5 and 2.5. Upstream blowing is then more robust as the maximum available control efficiency is higher.

For co-rotating configurations, it was found that the optimum of $\frac{\lambda}{\Phi}$ is 13.6, and for counter-rotating configurations, it was found that $\frac{\lambda}{\Phi}$ has to be smaller than $2\frac{L}{\Phi}$. It was also confirmed that the optimum value for $\frac{L}{\Phi}$ is between 12.3 and 16 and the configuration with $\frac{L}{\Phi} = 15$ and $\frac{\lambda}{\Phi} = 27.3$ is then a good compromise.

Finally the best $\frac{\Phi}{\delta}$ found is 0.03, as at constant VR, the configurations with the smaller diameter ($\frac{\Phi}{\delta} = 0.03$) tested give results comparable to the corresponding one with $\frac{\Phi}{\delta} = 0.06$ but with less flow rate.

Table 5 gives a summary of the optimum parameters for co and counter-rotating configurations found. The best of all configurations investigated is the counter-rotating one, $\frac{\Phi}{\delta} = 0.03$, $\frac{\lambda}{\Phi} = 27.3$, $\frac{L}{\Phi} = 15$ and $\alpha = 135°$ (in bold in Table 5).

Table 5. Optimum parameters for co and counter-rotating configuration tested.

	$\frac{\Phi}{\delta}$	β	α	$\frac{\lambda}{\Phi}$	$\frac{L}{\Phi}$	VR
co	0.03	45	45	13.6	-	2
	0.03	45	135	13.6	-	3.5
counter	0.03	45	45	27.3	15	2
	0.03	**45**	**135**	**27.3**	**15**	**3.5**

ACKNOWLEDGEMENTS

The authors would like to thank the European Communauty for their financial support under the contract AVERT/RTD REG/H.3(2006)A/142121. The International Campus on Safety and Intermodality in Transportation (CISIT) is also acknowledge for their financial support.

REFERENCES

Betterton, J. G., Hackett, K. C., Ashill, P. R., J.Wilson, M., Woodcock, I. J., Tilmann, C. P., and Langan, K. J. (2000). Laser doppler anemometry investigation on sub-boundary layer vortex generators for flow control, in: 10th intl. symp. on appl. of laser tech. to fluid mech. Lisbon.

Carlier, J. and Stanislas, M. (2005). Experimental study of eddy structures in a turbulent boundary layer using particule image velocimetry. *Journal of Fluid Mechanics*, 535(36):143–188.

Compton, D. and Johnston, J. (1991). Streamwise vortex production by pitched and skewed jets in a turbulent boundary layer. *AIAA paper*, 91-0038.

Cuvier, C., Braud, C., Foucaut, J., and Stanislas, M. (2010). Flow characterisation and parametric study of passive and active vortex generators on the lml-avert ramp. Technical report, AVERT.

Cuvier, C., Braud, C., Foucaut, J., and Stanislas, M. (2011). Characterization of a separated turbulent boundary layer for flow control purpose. *Seventh International Symposium on Turbulence and Shear Flow Phenomena, July 28 - 31, Ottawa*.

GadelHak, M. (2000). *Flow Control : passive, active and reactive flow management*. Cambridge.

Godard, G. and Stanislas, M. (2006a). Control of a decelerating boundary layer. part 1: Optimization of passive vortex generators. *Aerospace Science and Technology*, 10(3):181–191.

Godard, G. and Stanislas, M. (2006b). Control of a decelerating boundary layer. part 3: Optimization of round jets vortex generators. *Aerospace Science and Technology*, 10(6):455–464.

Lin, J. C. (1999). Control of turbulent boundary layer separation using microvortex generators. *AIAA Paper*, (99-3404).

Lin, J. C. (2002). Review of research on low-profil vortex generators to control boundary layer separation. *Progress in Aerospace Sciences*, 38:389–420.

Lin, J. C., Howard, F. G., and Bushnell, D. M. (1990). Investigation of several passive and active methods for turbulent flow separation control, in: 21st fluid dynamics, plasma dynamics and lasers conference. *AIAA*, (paper 90-1598).

Lin, J. C., Selby, G. V., and Howard, F. G. (1991). Exploratory study of vortex-generating devices for turbulent flow separation control, in: 29th aerospace sciences meeting, january 7−10, reno, nevada. *AIAA*, (paper 91-0042).

McManus, K. R., Joshi, P. B., Legner, H. H., and Davis, S. J. (1994). Active control of aerodynamic stall using pulsed jet actuators. *AIAA paper*, 94:2218.

Selby, G. V., Lin, J. C., and Howard, F. G. (1992). Control of low-speed turbulent separated flow using jet vortex generators. *Experiments in Fluids*, 12:394–400.